Laboratori Nazionali di Frascati

LNF-61/40 (1961)

G. Bologna, G. Diambrini, A. S. Figuera, U. Pellegrini, B. Rispoli, A. Serra, R. Toschi: A PAIR SPECTROMETER FOR ENERGIES UP TO 2 GeV.

Estratto dal: Nuclear Instruments, 12, 263 (1961)

NUCLEAR INSTRUMENTS AND METHODS 12 (1961) 263–277; NORTH-HOLLAND PUBLISHING CO.

A PAIR SPECTROMETER FOR ENERGIES UP TO 2 GeV

G. BOLOGNA, G. DIAMBRINI, R. TOSCHI†

C.N.E.N. – Laboratori Nazionali di Frascati

and

A. S. FIGUERA††, U. PELLEGRINI §, B. RISPOLI §§, A. SERRA

C.N.E.N. – Laboratorio Elettronica

Received 28 February 1961

A pair spectrometer, having the capacity of analyzing photon energies up to 2 GeV is described.

The optical properties of the instrument are examined by calculating the horizontal and vertical deviation matrices.

Further, the magnetic measurements that were made both inside and outside the magnet gap in order to obtain information on the electron trajectories, are described. The method used in calculating the trajectories is given. The calculated trajectories are compared with the ones obtained experimentally by means of the floating wire technique, a description of which is also given.

Last, the electronic devices used in the electron detection are described.

1. Introduction

An electron pair spectrometer has been developed chiefly with the purpose of determining the energy spectrum of the Frascati 1 GeV electronsynchrotron γ-ray beam and with characteristics such as to allow also various experiments on electrodynamics. The maximum measurable photon energy is 2 GeV.

The pair spectrometer consists of the following parts:

a. magnet, for the deflection of electron pairs;

b. vacuum chamber;

c. converter, in which the γ-rays produce the electron pairs;

d. scintillation detector telescopes and electronic equipment for the detection of electron pairs.

2. Description of the Instrument

2.1. MAGNET DESCRIPTION

Fig. 1 shows the magnet and the exit side of the vacuum chamber. The magnet is of the shell type, with the two flux return paths placed on both sides of the path of the γ-ray beam.

Fig. 2 shows a cross section of the upper yoke obtained with a plane parallel to the pole surfaces.

In contrast to the design of previous spectrometers[1,2]), the high momentum trajectories pass out of the field through the exit face of the magnet rather than a side. Hence there is essentially no focusing in the horizontal plane. With this design it is possible to keep the size of the instrument a minimum.

The technical details of the magnet are as follows:

Maximum induction in the gap:	20 kgauss
Iron quality:	T 11 S Terni, forged at low C content (30 KAT/m, 20 kgauss)
Iron weight:	17.8×10^3 kg
Magnet height:	1326 mm
Pole faces:	flat and parallel within $\pm$ 0.1 mm
Gap height:	100 ± 0.1 mm
Pole height:	15 mm
Excitation coil:	120 turns around each pole
Maximum current:	2100 A
Coil:	square copper bars (13.5×13.5) mm² with a central hole 7 mm in diameter
Winding weight:	0.75×10^3 kg
Resistance (at 70° C):	0.90 Ω
Inductance:	57 mH
Cooling water:	flow 1.3 l/s; pressure 3 kg/cm² .

† Now at C.N.E.N.-Laboratorio Gas Ionizzati, Frascati.

†† Now at the Physics Department, University of Maryland.

§ Now at LABEN, Milano.

§§ C.N.E.N.-Laboratorio Elettronica and Istituto di Fisica, Università di Roma.

[1]) K. M. Crowe and R. H. Phillips, Phys. Rev. 96 (1954) 470; K. M. Crowe, Thesis-Report UCRL 2050 (1952) (unpublished).

[2]) D. H. Cooper, Thesis-Cal. Inst. Techn. (1955) (unpublished).

The above characteristics are justified by the following considerations.

Owing to the high induction value required in the gap, the use of high poles must be avoided to prevent saturation at the pole bases; poles only 15 mm high have therefore been used. Because of the high induction value, and of the limitation of the number of turns possible, the current density in the coil must be very high (15 A/mm^2) and requires a considerable flow of cooling water. Due to the small coil window ((230 × 130)mm^2), the magnetic flux loss in this magnet is small. Thus the magnet weight (18.5 ton) is maintained to a minimum for the required stored energy.

Fig. 2 shows the holes bored in the upper yoke, which permit the introduction of the light pipes for scintillation detectors inside the magnet gap†. With the exception of two, these holes are set in pairs with their centers on circles which are tangential to the direction of the photon beam at the point C of the converter††. All the holes can be plugged when not used so as to restore the iron continuity; the plugs are flanged on the top and provided with a vacuum gasket.

† These counters have not been used to determine the bremsstrahlung spectrum of the electronsynchrotron.

†† Double coincidences for each branch of a pair may be obtained in this manner, and spurious counts generated by back scattering of the walls may mostly be eliminated.

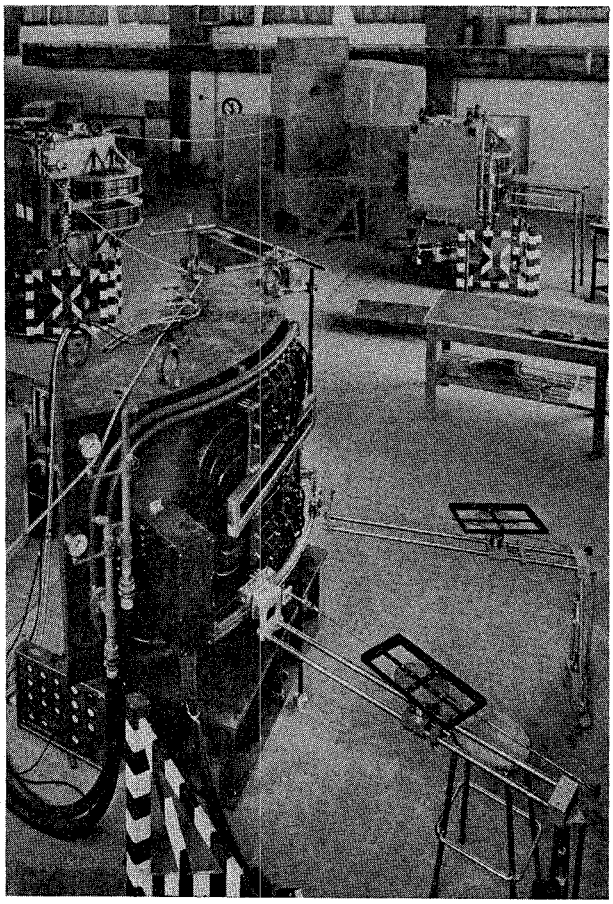

Fig. 1.
Pair spectrometer: the magnet and the vacuum chamber.

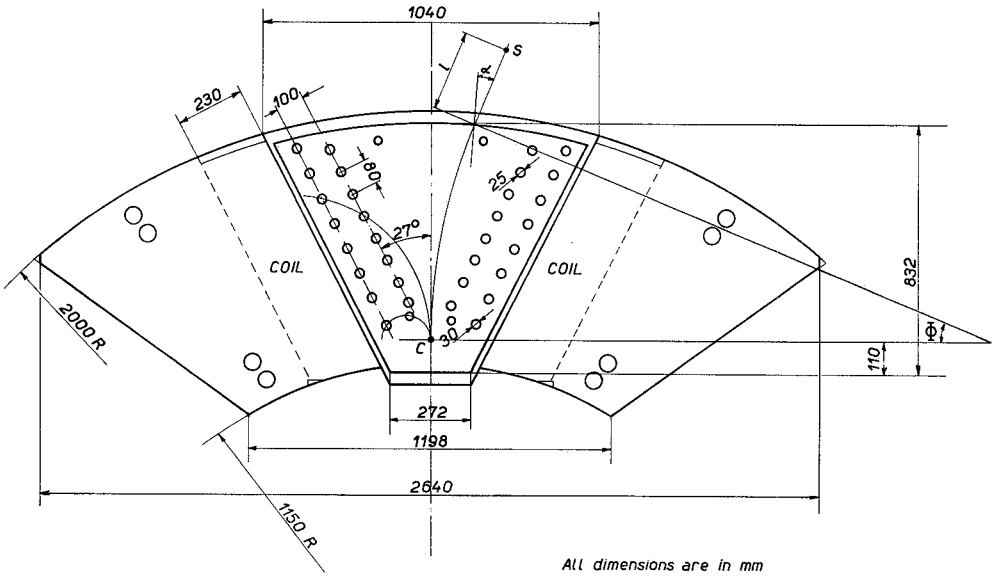

Fig. 2. Magnet: cross section of the upper yoke.

2.2. DESCRIPTION OF THE VACUUM CHAMBER

Fig. 1 shows the vacuum chamber projecting from the gap.

In fig. 3 the vacuum chamber can be seen laying on the lower yoke. It is made of stainless steel and consists of two walls connected by two flanges. This chamber is introduced into the space left between the poles when the upper yoke is lifted. The walls of the chamber are fitted in appropriate grooves made around the poles and provided with vacuum gaskets. The chamber is screwed to the lower and upper yokes. A vacuum of 0.03 mm Hg may be maintained with the help of a conventional rotary pump having a speed of 10^3 l/min. Since the polar faces were used as upper and lower chamber walls, we are not losing any height or precision in the gap.

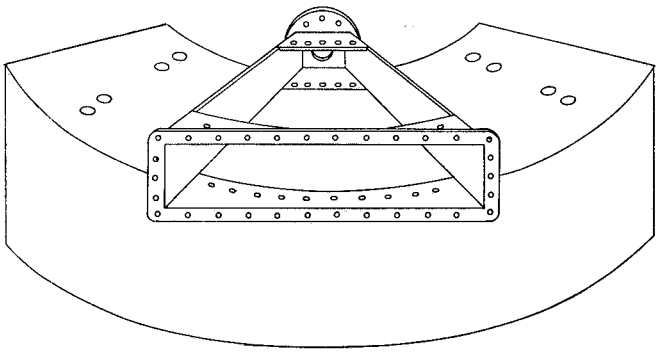

Fig. 3. Vacuum chamber.

Applied to the two flanges are: at the entrance a tube 15 cm in diameter, 4 m long, passing through a broom magnet to a collimator†, and at the exit a mylar foil 0.2 mm thick (equal to about 5×10^{-4} radiation lengths). The equivalent thickness of the residual air and of the mylar foil is so small that no background disturbances arise, owing to the characteristics of the counter telescopes (see section 7).

2.3. DESCRIPTION OF THE CONVERTERS – SPECTROMETER ALIGNMENT

We use three aluminum converters 1; 0.1; 0.01 mm thick, equal to 0.011; 0.0011; 0.00011 radiation lengths, respectively. They are applied to plexiglass rings, each having a diameter of 6 cm. The rings are mounted on a turntable which can be positioned remotely, so that they may be interposed in the path of the beam; each ring is automatically turned up within the beam when it reaches the proper position.

Fig. 4 shows one of these converters†† intercepting the γ-ray beam; the others are laying on the turntable and do not disturb the beam. On this device a place is reserved for a brass ring 3 mm thick, for adjusting the position of the beam and collimators. The initial alignment of the spectrometer along the γ-ray beam has been obtained by placing another brass ring, slightly larger in diameter than the one mentioned above, at the exit of the spectrometer, with its center on the spectrometer axis. The position of the spectrometer was adjusted so that the shadows of the two rings in a radiograph of the γ-ray beam appeared concentric. Thereafter, the spectrometer was no longer shifted and, in order to align the beam, one had to make little adjustments of the tantalum target inside the synchrotron and of the two collimators inserted in the γ-ray beam, until the photographed shadow of the first ring alone appeared centered on the beam.

3. Optical Properties of the Spectrometer

The optical properties of the spectrometer were determined during the design by calculating the

† The general experimental arrangement is described in other papers[3]).

†† The figure shows also another device used to control a monocristalline sylicon converter employed in an another experiment[4]). At present the single crystal is removed and does not disturb the beam. A scintillation detector used for the same experiment may also be seen.

[3]) G. Diambrini, A. S. Figuera, A. Serra and B. Rispoli, Nuovo Cimento 15 (1960) 500, and Nuovo Cimento 19 (1961) 250.

[4]) G. Bologna, G. Diambrini and P. G. Murtas, Phys. Rev. Letters 4 (1960) 134.

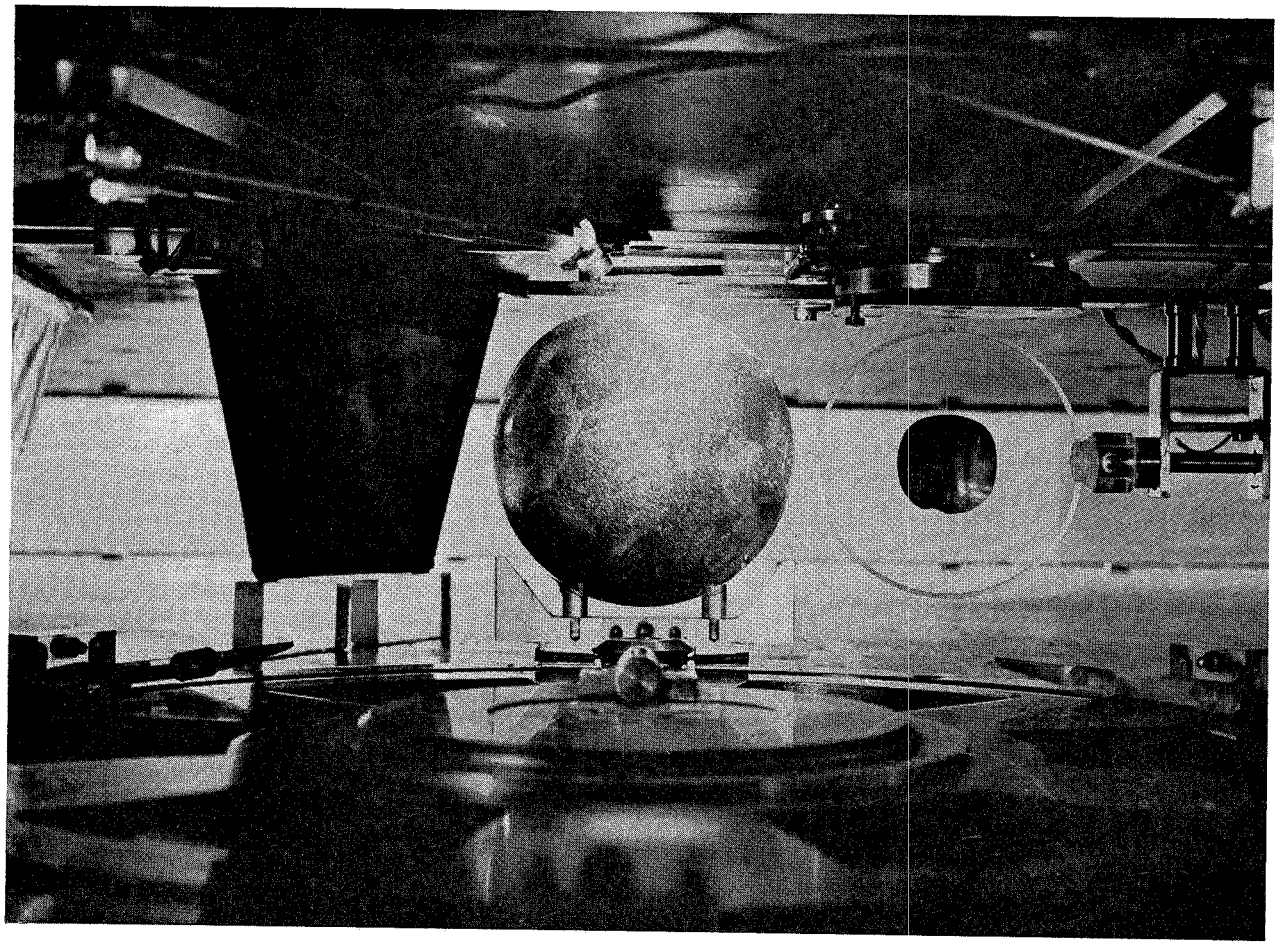

Fig. 4. View of the converter turntable, showing one aluminum converter in position.

matrix elements $H_{ij}(i, j, = 1, 2, 3)$; $V_{hk}(h, k = 1, 2)$ of the horizontal and vertical deflections in the Gauss linear approximation, obtained by resolving the equation of motion[5]). The field was assumed $B = \text{const.} \neq 0$ in the gap of the magnet, and $B = 0$ outside.

Let us consider an electron of momentum p emerging from the center C of the converter and directed, initially, along the spectrometer axis; the trajectory lies in the median plane (M.P.), which is horizontal. Let r be the radius of curvature of that portion of the trajectory internal to the spectrometer; ϕ be its deflection angle; α be the angle between the trajectory and the normal to the edge of the spectrometer; l be the distance of a point S from the edge, measured along the trajectory—point in which will be placed the center of the first detector (see fig. 2). We shall call this the principal trajectory.

The quantities r, ϕ, α are assumed positive for all trajectories bending to the right of the spectrometer axis and negative for those to the left. Let $p + \Delta p$ be the momentum of an electron which emerges from the point (ξ_0, ζ_0) of the convertor, measured with respect to the point C. The coordinates (ξ, ζ) of this electron at the detector, relative to the point S are given by

$$\begin{pmatrix} \xi \\ \xi' \\ \Delta p/p \end{pmatrix} = \begin{pmatrix} H_{11} & H_{12} & H_{13} \\ H_{21} & H_{22} & H_{23} \\ H_{31} & H_{32} & H_{33} \end{pmatrix} \begin{pmatrix} \xi_0 \\ \xi'_0 \\ \Delta p/p \end{pmatrix}$$

$$\begin{pmatrix} \zeta \\ \zeta' \end{pmatrix} = \begin{pmatrix} V_{11} & V_{12} \\ V_{21} & V_{22} \end{pmatrix} \begin{pmatrix} \zeta_0 \\ \zeta'_0 \end{pmatrix}.$$

[5]) P. G. Sona, Internal note no. 3 (1958) – I.N.F.N., Laboratori Nazionali di Frascati.

The primes signify the derivative with respect to s, the distance measured along the principal trajectory. Then we have:

$$
\begin{aligned}
H_{11} &= \left(1 + \frac{l}{r}\tan\alpha\right)\cos\phi - \frac{l}{r}\sin\phi \\
H_{12} &= r\left(1 + \frac{l}{r}\tan\alpha\right)\sin\phi + l\cos\phi \\
H_{13} &= r\left(1 + \frac{l}{r}\tan\alpha\right)(1 - \cos\phi) + l\sin\phi \\
H_{21} &= \frac{l}{r}(\tan\alpha\cos\phi - \sin\phi) \\
H_{22} &= \tan\alpha\sin\phi + \cos\phi \\
H_{23} &= \tan\alpha\,(1 - \cos\phi) + \sin\phi \\
H_{31} &= H_{32} = 0\,; \qquad H_{33} = 1\,.
\end{aligned} \tag{1}
$$

$$
\begin{aligned}
V_{11} &= 1 - \frac{l}{r}\tan\alpha \\
V_{12} &= \left(1 - \frac{l}{r}\tan\alpha\right)r\phi + l \\
V_{21} &= -\frac{l}{r}\tan\alpha \\
V_{22} &= 1 - \phi\tan\alpha\,.
\end{aligned} \tag{2}
$$

Since the spectrometer has a symmetry plane, horizontal and vertical deviations are quite independent and decoupled, so that we may take them into account separately.

3.1. DEVIATION IN THE HORIZONTAL PLANE

The following factors influence the dispersion and resolving power:

1. Finite width of the converter and angular spread of the γ-ray beam.

2. Multiple scattering of the particles in the converters and pair emission angle different from zero.

3. Energy loss by ionization and radiation of the particles in the converter.

Let us consider an electron having a momentum $p + \Delta p$, emerging from C in the direction of the principal trajectory. Let us call this new trajectory "varied".

The dispersion and resolving power are given, respectively, by:

$$
D = \frac{\xi}{\Delta p} = \frac{|H_{13}|}{p}
$$

$$
P = \frac{p}{\Delta p} = \frac{|H_{13}|}{\xi}\,. \tag{3}
$$

Let us show now that the first factor cited above does not introduce any aberration, as far as the measurement of the γ-ray beam energy spectrum is concerned. As may be seen later on (see section 7), only one counting channel is being used and it consists of two counter telescopes placed in a symmetrical position with respect to the spectrometer axis; the detectors are placed perpendicularly to the principal trajectory passing through their center. Let us assume that the cross section of the γ-ray beam at the converter is circular with a radius c (we shall call $2c$ the "width" of the converter) and that 2ω is the angular spread of the beam. Let $2a$ be the width of the first detector of each telescope. At point P_- of the detector, a distance ξ from point $S_- \equiv S$, the momentum spread of an electron leaving the edge of the converter in the same direction as the creating photon, is:

$$
\frac{\delta_- p}{p} = \frac{\xi_- \mp cH_{11} \mp \omega H_{12}}{H_{13}}\,.
$$

Let us assume that the positron created simultaneously with the preceding electron crosses the detector in a point P_+, ξ_+ distant from S_+, symmetric point of S_-, with respect to the spectrometer axis. Taking into account the algebraic signs of r, ϕ, and α, we have from (1):

$$
\frac{\delta_- p}{p} + \frac{\delta_+ p}{p} = \frac{\xi_-}{H_{13}} - \frac{\xi_+}{H_{13}}\,,
$$

H_{13} being relative to S_-; therefore we obtain the algebraic sum of the momentum spreads that we would have for the principal trajectories. This means that, *in linear approximation*, the photon is detected as it passed through the center of the converter directed exactly as the axis of the spectrometer, i.e. as if the source were a point.

It is useful to calculate the maximum angle β between the principal trajectory and the one leaving from the edge of the converter, when they cross the first detector: this angle enables us to calculate the dimensions that the following detectors should

have in order to collect all the electrons passing through the first detector†.

We obtain:

$$\beta = \frac{H_{23}}{H_{13}}(a + cH_{11} + \omega H_{12}) - (cH_{21} + \omega H_{22}) . \quad (4)$$

As far as the second factor is concerned, we can say that the aberrations caused by the multiple scattering and by the emission angle of the electrons in the converter modify the triangular resolution function of the detectors[2]). With the thickness of the converters now used and at the energies that concern us, this effect may be neglected as compared with the aberrations produced by the same causes in the vertical plane. In such cases the ionization and radiation energy losses in the converter are also negligible.

3.2. DEVIATION ON THE VERTICAL PLANE

The limiting angles with respect to the spectrometer axis, at which an electron can be emitted in the vertical plane at a height z above the M.P., so that it may be collected by the first detector, $2h$ in height, are given by:

$$\theta_{l_{1,2}} = \frac{1}{V_{12}}[\pm h - zV_{11}] , \quad (5)$$

with $|z| < c$.

Taking these angles into account, we may determine the vertical counting losses due to the multiple scattering and the emission angle of the electrons, as a function of the photon energy and of the converter and detector heights. The calculation is given in the second paper of ref.[3]).

The maximum γ angle defined similarly to the β angle, but in the vertical plane is given by:

$$\gamma = \frac{V_{22}}{V_{12}}[h + cV_{11}] - cV_{21} . \quad (6)$$

3.3. APPLICATION TO OUR TELESCOPES

For the counting channel being used we took:

$$r = 1.67\,m \qquad l = 1\,m$$
$$\phi = 26°30' = 0.464\,\text{rad} \qquad \alpha = 21°50' . \quad (7)$$

† Actually one should also take into account the multiple scattering in the detectors.

We therefore obtain from (1) and (2):

$$\| H_{ij} \| = \begin{pmatrix} 0.84 & 1.82 & \mp 0.67 \\ -0.054 & 1.07 & \mp 0.49 \\ 0 & 0 & 1 \end{pmatrix}$$

$$\| V_{hk} \| = \begin{pmatrix} 0.76 & 1.59 \\ -0.24 & 0.81 \end{pmatrix} , \quad (8)$$

with the upper or lower algebraic sign, depending on whether it concerns point S of fig. 2 or its symmetrical with respect to the spectrometer axis. From the value of V_{11}, which represents the linear vertical magnification, we deduce that, for $l = 1$ m, the spectrometer has weak focusing properties on the vertical plane.

From (3) we obtain:

$$\frac{1}{pD} = \frac{\Delta p/p}{\xi} = 1.5\,\%/\text{cm} . \quad (9)$$

As can be seen from section 7 and from ref.[3]), we have:

$$2a = 1.8\,\text{cm} \qquad 2h = 5.4\,\text{cm}$$
$$2c = 5.3\,\text{cm} \qquad 2\omega = 3.6\,\text{mrad} . \quad (10)$$

We obtain therefore from (4) and (6):

$$\beta = 25\,\text{mrad}$$
$$\gamma = 31\,\text{mrad} . \quad (11)$$

Further, we have from (5):

$$\theta_{l_{1,2}} = [\pm 17.7 - 4.78z] \times 10^{-3}\,\text{rad} , \quad (12)$$

z being measured in cm.

4. Magnetic Measurements

4.1. GENERAL CONSIDERATIONS

It is very likely that the assumption of a step function field, although sufficient for the calculation of the deviations from the principal trajectory, i.e., of the matrices $\| H_{ij} \|$, $\| V_{hk} \|$, does not apply to the calculation of the principal trajectory itself.

A better approximation could be obtained by substituting the mechanical length of the magnet by its "magnetic" length, thus taking into account also the fringing field.

For this purpose it is necessary to measure the behaviour of the magnetic field. We preferred to have the measurements analyzed directly by an

electronic computer, so as to obtain a higher precision. As one may see in section 5, the computation has given us both the principal and the varied trajectories. As a further check, these trajectories have been compared with the ones obtained by means of the floating wire technique (see section 6).

For determining the principal trajectories it is sufficient—owing to the existence of a symmetry plane—to determine the distribution B_z of the field component perpendicular to the M.P. on the M.P. itself. The B_z distribution ought to be measured with several excitation currents, but since it was observed that at the converter center C the field is a linear function of the current, at least up to 15 kgauss, we assumed that the B_z distribution, with respect to the value B_c at the converter, was independent of the excitation current. The measurements were therefore taken when the value B_c was 10 kgauss.

Different methods were employed for the inner and outer positions.

4.2. MEASUREMENTS INSIDE THE GAP

Inside the gap we measured the relative difference of magnetic field:

$$\rho = \frac{B_z - B_c}{B_c} = \frac{\Delta B}{B_c} \qquad (13)$$

B_z being the vertical component of the field (coincident now with the field itself) existing at a certain position in the M.P. and $B_c = 10$ kgauss the field existing at the center C of the converter.

The measurements were performed with an electronic fluxmeter of the Dicke type[6]) and a coil, 12 mm in diameter and 20 mm in height. The coil dimensions are justified by the field homogeneity (see later on). In the tested region the coil electric axis always coincides with its geometrical axis.

In order to determine the coil position, we used a plexiglass plate, fitted to the lower pole. On it we made a square grid of holes, in which the coil support could be inserted. The centers of the holes were spaced by 1 cm. The geometric center of the coil was always on the M.P. within $\pm$ 0.1 mm, its axis being vertical within $\pm$ 30′.

[6]) G. Diambrini and G. Ghigo (to be published).

In order to obtain ρ, the flux variation corresponding to ΔB was measured by moving the coil on the plate and that corresponding to B_c by rotating it through 180° $\pm$ 30′, at C. With such an angular uncertainty the measurements of the vertical components was achieved with an error lower than $\pm$ 0.05%.

During the measurements the excitation current was maintained stable within $\pm$ 0.1%, but the field fluctuations were, however, still of the order of ΔB. Hence we tried to compensate them by means of a fixed coil connected to the movable one, and identical to it, in such a way that the flux variations with time tend to compensate one another. Thus the error in the determination of ΔB could be maintained within $\pm$ 1 gauss. To minimize the fluxmeter error we always used the same scale. In order that the instrument indication corresponding to ΔB and B_c had about the same value, in measuring B_c, we used a resistive divider, from which one may derive a convenient fraction (having an error of $\pm$ 0.1%) of the voltage induced at the coil ends.

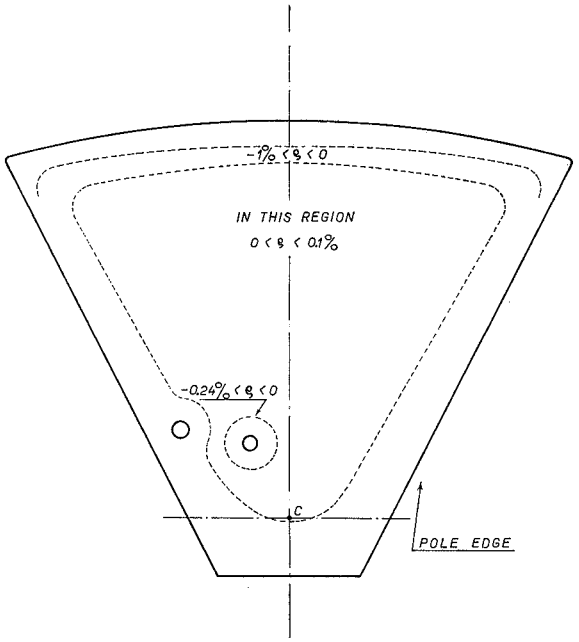

Fig. 5. Plot of the magnetic field distribution. The variation of the field within several regions is indicated.

Taking into account all the errors, the maximum absolute error in the determination of $\delta\rho$ is:

$$\delta\rho = \pm\ 0.0001\ .$$

In the central region of the gap, where the magnetic field varies little, the distance between two successive measurements was 5 cm; towards the edges, where the field variation is stronger, steps of 1 cm was chosen. There were 600 measurements altogether.

Fig. 5 shows the results; it indicates the M.P. regions inside of which ρ lies between the values written in the figure. At the point C we determined the dependence of the magnetic field upon the excitation current by using a nuclear magnetic resonance method[7]). The error in the field measurement was $\pm$ 0.02%; the one in the current $\pm$ 0.1%.

4.3. MEASUREMENTS OUTSIDE THE GAP

Towards the edge of the magnet the use of the fluxmetric method previously mentioned did not prove convenient, inasmuch as the magnetic field variation is no longer linear with the displacement and it is therefore difficult to ascertain the exact position of the coil electric axis. Further, the use of a coil outside the magnet requires too much time.

We have therefore used a Hall probe[8]) of 11 $\times$ 3 $\times$ 1 mm^3 in size. A 150 mA current, stabilized within $\pm$ 0.1%, supplied by a current generator, was sent to one electrode pair. The other electrodes, which supplied the Hall voltage, were connected to a suitable resistor, with the purpose of linearizing the probe output. The voltage across the terminals of this resistor was measured with a L & N K3 potentiometer. The probe had previously been calibrated with the nuclear magnetic resonance method. An error of $\pm$ 0.1% was included, due to the Hall constant variation with the temperature.

The probe was mounted on an appropriate arm that enabled us to introduce it up to where the magnetic field did not differ more than 0.1% from the value B_c. In view of the circular sector shape of the magnet, it proved convenient to move the probe on the M.P. along straight lines converging at the curvature center. Measurements were made along 16 radial lines; altogether 600 points were tested.

Fig. 6 shows the behaviour of the ratio (measured along the spectrometer axis)

$$\sigma = \frac{B_z}{B_c}. \tag{14}$$

Bearing in mind all the causes of error described above, we can say that the maximum error in the determination of σ was

$$\frac{\delta\sigma}{\sigma} = \pm\, 0.3\,\%\,.$$

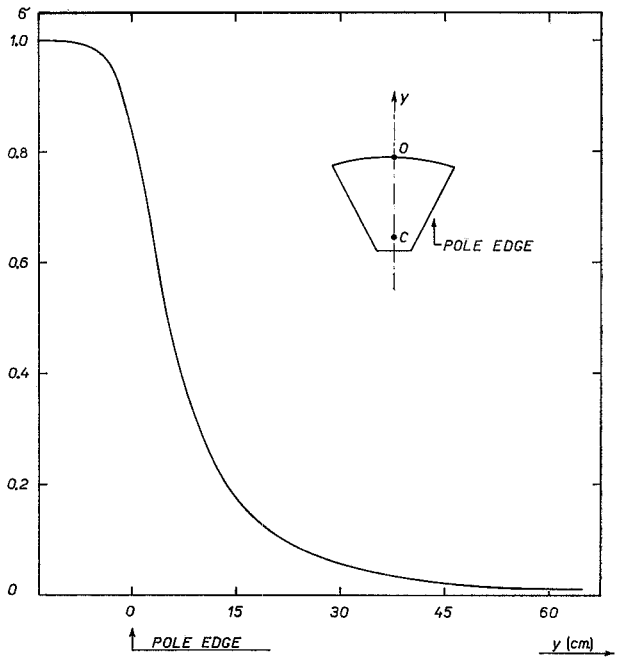

Fig. 6. Results of the magnetic measurements outside the gap, along the spectrometer axis.

From fig. 6 one can deduce that the equivalent magnetic length along the spectrometer axis exceeds the mechanical length of the magnet by an amount of 8.7 $\pm$ 0.1 cm. In the other useful directions, the variation of σ never exceeds $\pm$ 0.005. This figure corresponds to a variation of the magnetic length less than $\pm$ 0.3 cm.

5. Calculation of the Trajectories

5.1. GENERAL CONSIDERATIONS

The particle trajectories have been obtained from the magnetic measurements with an electronic computer†.

[7]) G. Bologna, Thesis – (1955) (unpublished).
[8]) J. L. Symonds, Rep. Progr. Phys. **18** (1955) 83.
[9]) G. Pesamosca, Thesis – (1960) (unpublished).

† The magnetic measurement data and the equations for the principal and varied trajectories were programmed by Dr. G. Pesamosca[9]) on the Ferranti electronic computer of the Instituto Nazionale per le Applicazioni del Calcolo – Roma.

For the principal trajectories the differential equation of motion to be integrated is[1]):

$$\frac{d^2y}{dx^2} = \frac{\left[1 + \left(\frac{dy}{dx}\right)^2\right]^{\frac{3}{2}}}{r(x, y)}$$

$$r(x, y) = \frac{pc}{eB_z(x, y)}, \qquad (15)$$

y being the cartesian coordinate directed along the spectrometer axis and x the other rectangular coordinate; the origin is fixed at point C of fig. 2.

In view of its numerical resolution, the Milne method was adopted, using as a starting method the Runge-Kutta method[10]).

For the varied trajectories the Kerst-Serber equations[11]) were used:

$$\frac{d^2\xi}{ds^2} + [1 - n(s)]\frac{\xi}{r^2(s)} = \frac{1}{r(s)}\frac{\Delta p}{p}$$

$$\frac{d^2\zeta}{ds^2} + n(s)\,\zeta = 0, \qquad (16)$$

s being the curvilinear abscissa on the principal trajectory, ξ and ζ being, respectively, the deviations on the horizontal and vertical planes of the varied from the principal trajectory, $n(s)$ being the field index defined by:

$$n(s) = -\left[\frac{\partial B_z(s)}{\partial \xi}\right]_{\xi,\,\zeta\,=\,0}\frac{r(s)}{B_z(s)}$$

and $B_z(s)$ being the vertical component of the field on the principal trajectory.

Equations (16) hold in the Gauss linear approximation, i.e.:

$$|\xi| \ll r \qquad |\zeta| \ll r$$

$$\left|\frac{d\xi}{ds}\right| \ll 1 \qquad \left|\frac{d\zeta}{ds}\right| \ll 1.$$

Both the Milne and Runge-Kutta methods were used to solve equations (16), after having made the substitution:

$$s(x) = \int_0^x \left[1 + \left(\frac{d^2y}{dt^2}\right)^2\right]^{\frac{1}{2}} dt.$$

The field index $n(s)$ was evaluated along the principal trajectory from the measurements of $\Delta B_z/B_z$ nearby.

5.2. RESULTS

The integration error in (15) and (16) was estimated as being less than the one due to the experimental errors in the magnetic measurements. The error propagated from these latter to the momentum value corresponding to a principal trajectory is:

$$\frac{\delta p}{p} = \pm\, 0.15\,\%.$$

Once calculated, the principal trajectories were compared with the ones obtained by means of the floating wire technique (see section 6).

Five varied trajectories were then calculated, three of which were horizontal and two vertical, i.e. the ones required for the calculation of the matrix elements (1), (2). The varied horizontal trajectories were calculated also as principal trajectories, by using (15). A comparison with the trajectory obtained by means of the first of (16) showed perfect agreement.

We obtained:

$$\| H_{ij} \| = \begin{pmatrix} 0.824 & 1.779 & \mp\, 0.678 \\ -\,0.0639 & 1.075 & \mp\, 0.525 \\ 0 & 0 & 1 \end{pmatrix}$$

$$\| V_{hk} \| = \begin{pmatrix} 0.790 & 1.573 \\ 0.226 & 0.815 \end{pmatrix}. \qquad (17)$$

We note the good agreement between these values and the ones given by (8), calculated in the step function field approximation.

Naturally, the values given by (17) are the more reliables ones, according to which the various quantities of section 3 may be calculated once more.

We obtain:

$$\frac{\Delta p/p}{\xi} = 1.47\%/\text{cm}$$

$$\beta = 26 \text{ mrad}$$

$$\gamma = 31 \text{ mrad}$$

$$\theta_{l_{1,2}} = [\pm 17.2 - 5.02z] \times 10^{-3} \text{ rad}. \qquad (18)$$

[10]) F. B. Hildebrand, Introduction to numerical analysis (MacGraw-Hill, New York, 1956).

[11]) D. W. Kerst and R. Serber, Phys. Rev. **60** (1941) 53.

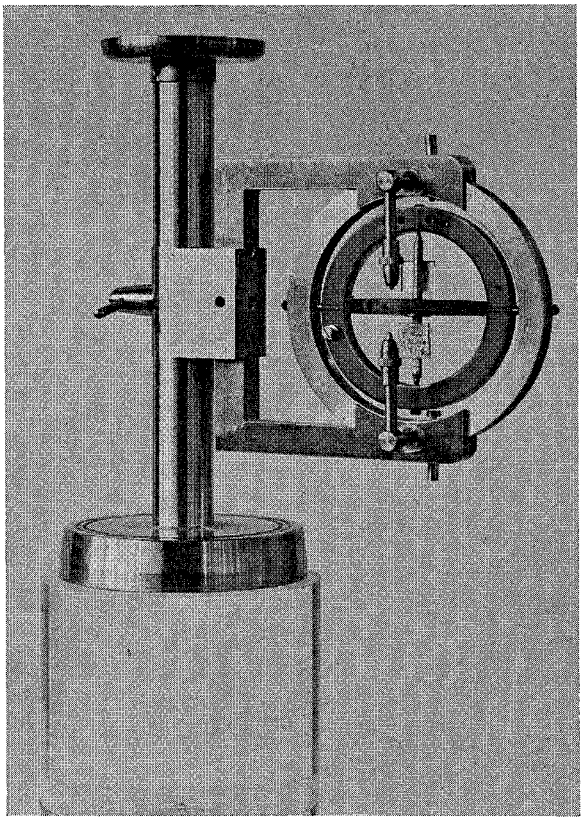

Fig. 7a.

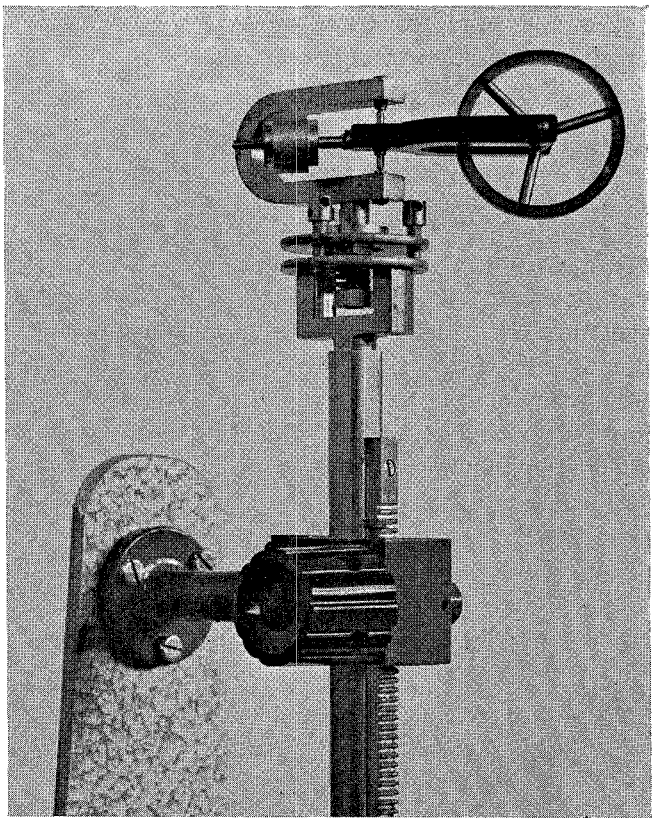

Fig 7b.

Fig. 7a, 7b. Devices employed in the measurements performed with the floating wire technique.

6. The Floating Wire Technique

6.1. DESCRIPTION OF THE APPARATUS. MEASUREMENT METHOD

The floating wire technique[8]) has been employed with a view to determining the position to be assigned to the counter telescope when the trajectories—calculated by means of the electronic computer—were not yet known. Some of the matrix elements (1) and (2) were also determined.

We used the devices of fig. 7.

Fig. 7a shows two araldite wheels, the inner one having its rotation axis perpendicular to its plane, while the outer has it coplanar. The two axes are coplanar and perpendicular to each other. The whole system is supported by an external brass ring, by two arms and by a support which may be wedged between the spectrometer poles. The inner wheel has an external diameter of 2.4 cm; two small mirrors are affixed to its axis: only the upper mirror is used, while the lower one serves for balancing the system.

The system is built in such a way as to be in neutral equilibrium; 1 mg applied to one of the wheels will suffice to unbalance it. The materials used are all diamagnetic; the bearings are made of tungsten.

The copper wire used in the measurements, 0.08 mm in diameter, is clamped in a hole bored in the rim of the internal wheel. Two silver wire segments, 1 cm long and 0.02 mm in diameter are soldered to the copper wire at the wheel; their ends are connected to the two vertical terminals shown in fig. 7a, so as to allow the pulley to be rotated about 30°.

The whole system was wedged between the poles in such a position that the point of the internal wheel, where the wire was secured, could be moved along a vertical line passing through C.

The wire passes through the magnet gap and

then passes to the pulley of the device shown in fig. 7b, which is built according to criteria similar to the preceding ones and placed outside the gap, in about the same position as the counter telescopes. The tension applied to the wire was 30 g. The wire could be supplied with a maximum current of 0.5 A without the danger of breaking.

The device shown in fig. 7a allows the wire to move freely both vertically and horizontally. In order to determine its position from outside the spectrometer, a light beam is sent, by means of a projector, to the posterior mirror seen in fig. 7a. The image is projected on an suitable screen. At first, with no current on, the wire is placed coincident with the spectrometer's axis, and the position of the light spot is observed.

In order to determine a principal trajectory in a certain field, the wire is supplied with the required current and the device seen in fig. 7b is moved until the spot comes back to its initial position.

Under these conditions the wire emerges (with a certain curvature) tangent to the spectrometer axis from the position corresponding to the converter center.

A varied trajectory may also be determined by either slightly changing the wire current, or by changing the emergency position of the wire or, last, by assigning a certain angle, measurable by the displacement of the light spot, to the initial direction of the wire.

6.2. DISCUSSION OF MEASUREMENT ERRORS

The following considerations may be made as regards possible measurement errors: by moving the device of fig. 7b vertically and horizontally and by taking it back to the initial position, the pulleys of fig. 7a return to their initial position with an error $\delta\theta = \pm 1$ mrad, both on the horizontal and vertical planes. The error propagated in the momentum measurement is then:

$$\frac{\delta' p}{p} = \frac{H_{12}}{H_{13}} \delta\theta \simeq \pm 0.26\% \, .$$

As a confirmation, we can say that a minimum weight of 70 mg had added to or subtracted from the initial 30 g to observe a motion of the light spot. This means a momentum variation of $\pm 0.23\%$.

The quota error in determining the position of the detector center is:

$$\delta'\zeta = V_{12}\, \delta\theta \simeq \pm 1.6 \text{ mm} \, .$$

By varying the field from 0 to 10 kgauss, with no current in the wire, the external wheel of fig. 7a rotates around its horizontal axis ± 1 mrad, owing to ferromagnetic impurities contained in the internal wheel axis. However there is no horizontal wire motion. The wire weight produces negligible effects, owing to the small deviation (less than 1 mm) from an horizontal plane.

The constraint imposed by the silver wire segments to the internal wheel is negligible because the segments have the same length and the same current flows in opposite directions. During the measurements we set the wires as symmetrically as possible with respect to the spectrometer axis.

The last error source is the uncertainty in the current determination, which is measured by the L& N K3 potentiometer, with an error of $\pm 0.05\%$.

Bearing all these errors in mind we may say that the momentum determination uncertainty amounts to:

$$\frac{\delta p}{p} = \pm 0.3\% \qquad (19)$$

and that the maximum error in the vertical coordinate of the wire with respect to the M.P. is:

$$\delta\zeta \simeq \pm 3 \text{ mm} \, . \qquad (20)$$

6.3. EXPERIMENTAL RESULTS

Measurements of principal trajectories were made with a magnetic field of $B_c = 10$ kgauss for a momentum $p = 500$ MeV/c (with a wire tension $F = 30$ g). The trajectory deviation from the M.P. was found to be less than 1 mm. The wire configuration in the horizontal plane was recorded on sensitive drawing paper; later on this was compared with the one obtained by means of the electronic computer, and the deviations were found to be in accordance with the experimental errors.

Further, the magnetic field and, at the same time, the wire current were varied so as to measure the momentum corresponding to the same wire configuration.

The results obtained are shown in the following table:

Momentum p(MeV/c)	Current in the wire (mA)	Field B_c (gauss)	B_c/p $\left(\frac{\text{gauss}}{\text{MeV}/c}\right)$
500	176.3	9943	19.89
450	195.9	8914	19.81
400	220.4	7951	19.88
350	251.9	6964	19.90
300	293.9	5966	19.89
250	352.7	4963	19.85

From the above table it may be seen that the ratio between the magnetic field and the momentum remains constant within the experimental errors.

A vertical varied trajectory was then measured, with the wire starting parallel to and 1 cm above the principal trajectory; the elevation at the detector was 0.7 cm; thus we have:

$$V_{11} = 0.7\,, \tag{23}$$

which is in good agreement with (17), and better than one would expect from (20).

Last, we measured the varied vertical trajectory starting from the converter center and forming with the principal trajectory an angle of 10 mrad; a rise of 23 mm was found at the first detector. Thus we have:

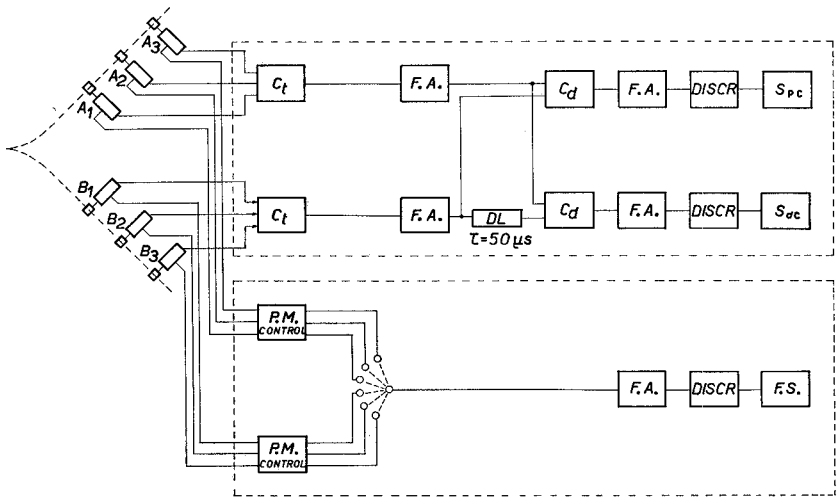

Fig. 8. General block diagram of the electronic apparatus.

Determinations of varied trajectories were then made; an increment Δi was given to the current and the distance ξ by which the wire was displaced, at the position of the first detector, was measured. We found:

$$\frac{\Delta p/p}{\xi} = 2.3\,\%/\text{cm}\,. \tag{21}$$

Taking into account formula (19) and the error in ξ ($\pm$ 0.3 mm), we may conclude that (18) and (21) agree.

As a result of (21) we have:

$$H_{13} = \pm\, 0.43\ \text{m}\,. \tag{22}$$

$$V_{12} = 2.3\ \text{m/rad}\,. \tag{24}$$

Taking into account the usual errors, this is in agreement with (17). It is reasonable to expect considerable differences between the results found by the wire and those obtained by the electronic computer. It should be borne in mind that these errors are determined by small increments in current and position. Naturally, the most reliable values are the ones obtained by means of the electronic computer.

The values (23) and (24) were used to determine the limiting angles (5) in the work on the γ-ray spectrum (see ref.[3]), at the time when the results of the computer were not yet known.

7. Apparatus for Detecting Electron Pairs

7.1. GENERAL BLOCK DIAGRAM

For detecting electron pairs of a certain energy, one channel has been used, with the detectors outside of the magnetic field.

A block diagram of the detectors and electronics is sketched in fig. 8. The channel consists of two telescopes of scintillation counters placed along the trajectories of the positive and negative electrons, having the same energy (symmetric pairs). Each telescope consists of three counters, the first of which is roughly at 1 meter from the magnet edge. This distance is determined by the conditions established for the spectrometer resolution.

The output pulses of the photomultipliers from both the anode and the last dinode are sent separately to two different electronic channels.

The outputs from the photomultipliers anodes of each telescope are sent to the input of a triple coincidence (C_t). The outputs of the two triple coincidence go, through a fast distributed amplifier (F.A.), to two double coincidences channels (C_d), giving both prompt and delayed coincidences (delay time $\tau = 50\ \mu s$) recorded by scalers S_{pc} and S_{dc}.

The outputs of dynodes are sent to a second electronic chain which enables us to check the behaviour of the detectors during the measurements. This chain consists of a fast distributed amplifier, a fast discriminator with a dead time of 100 ns, and a fast scaler (F.S.) with a resolution time of 50 ns.

7.2. DESCRIPTION OF THE DETECTORS

Each counter consists of a plastic scintillator, a light pipe, and a photomultiplier. The sizes of the plastic scintillators to obtain a momentum resolution $\Delta p/p \simeq 2.7\%$ were:

Scintillators $A_1 - B_1$ (18 × 54 × 1) mm³;
Scintillators $A_2 - B_2$ (40 × 76 × 1) mm³;
Scintillators $A_3 - B_3$ (72 × 106 × 1) mm³;

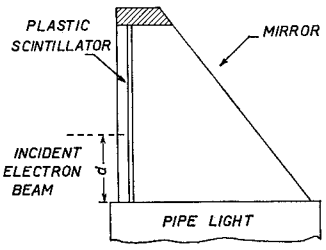

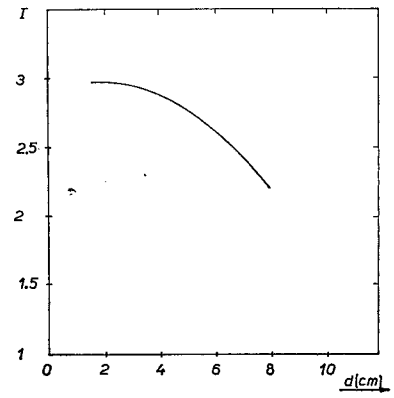

Fig. 9. On the left: Geometry of the detectors. On the right: Intensity of the collected light (arbitrary units) vs. the distance of the point of incidence from the edge of the scintillator.

In order to obtain a reasonable response uniformity from the scintillator and the best light collection, we used the geometry of fig. 9, placing the scintillator in optical contact with the pipe-light.

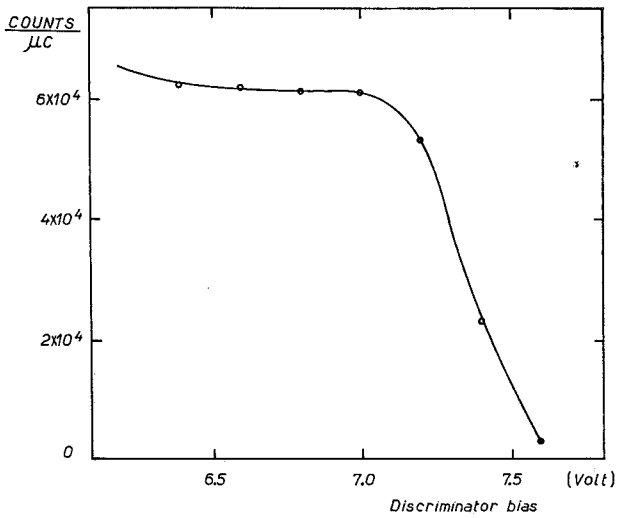

Fig. 10. Counting rate of the 1–2 double coincidence channel of the triple coincidence vs. delay time.

In the same figure the efficiency of light collection is plotted versus the distance of the point of incidence from the near edge of the scintillator.

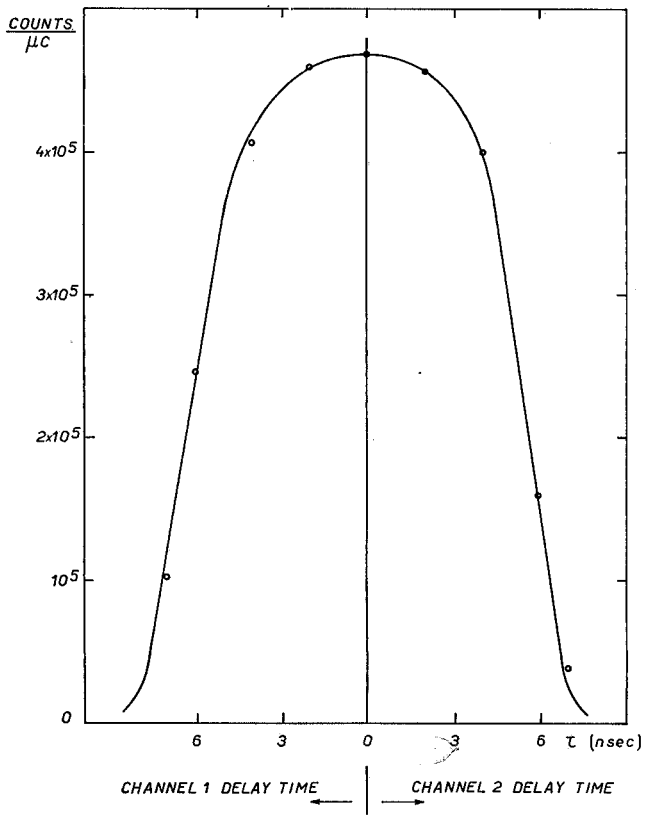

Fig. 11. Counting rate of the triple coincidence as a function of the discriminator voltage level.

The photomultipliers used are of the RCA 6810A type. Supply voltage and potentials partition for dynodes and focusing as well as accelerating grids are so chosen in order to obtain the same gain for the six P.M.

In the actual measuring conditions all the various coincidence channels are fed with signals having an amplitude greater than 5 V.

Magnetic shielding is given by two cylinders: the inner one of μ-metal and the external one of soft iron 0.5 cm thick.

7.3. CHARACTERISTICS OF THE ELECTRONIC APPARATUS

Triple coincidences are of the line type with distributed constants, which have been already described[12]). The resolution time was fixed at 6 ns. Fig. 10 shows the characteristic of the 1–2 double channel of the triple.

In fig. 11 the number of counted events is plotted against the level of the discriminator inside the coincidence.

[12]) U. Pellegrini, B. Rispoli and A. Serra, Nuovo Cimento **9** (1958) 171.

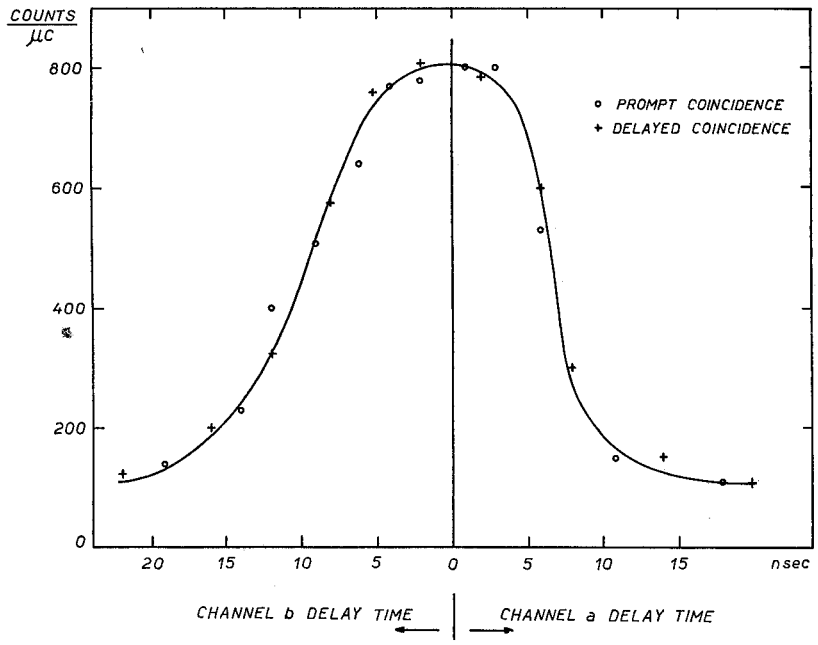

Fig. 12. Counting rate of the double coincidence vs. delay time.

The signals incoming from the two triple coincidences trigger the first double coincidence and the second one after a time shift of 50 ns. From the output of the first coincidence we take the simultaneous coincidences, while from the output of the second one we get the delayed one. The coincidence characteristics drawn in fig. 12 and in fig. 13 have the same shape for the two double circuits.

With a view of avoiding possible integration effects, we placed at the output of both double coincidence circuits distributed amplifiers followed by trigger circuits having the input sensitive to fast pulses 20 ns long.

The scalers following the discriminators are of the conventional type, having 1 μs as resolution time.

This electronic assembly has been working continuously more than 600 hours without any trouble.

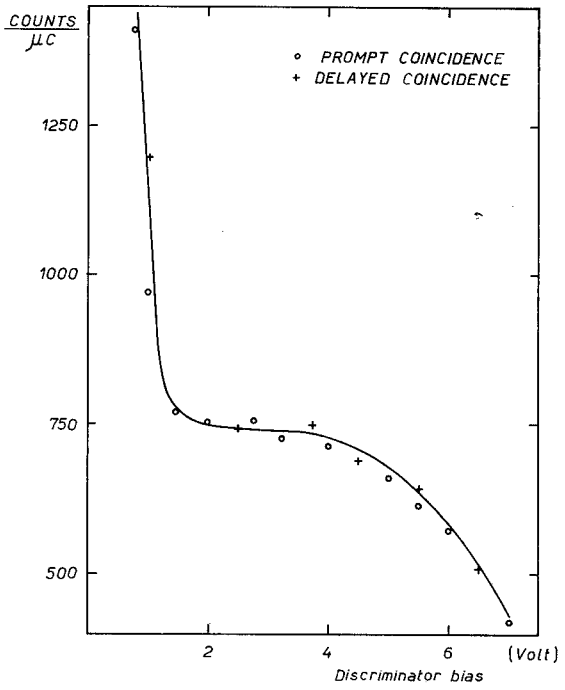

Fig. 13. Counting rate of the double coincidence as a function of the discriminator voltage level.

One of us (G.B.) is very indebted to Prof. J. De Wire for helpful discussion.